Aalborg Universitet

AALBORG UNIVERSITY

A Wideband Filtering Antenna Array with Harmonic Suppression

Zhang, Yiming; Zhang, Shuai; Yang, Guangwei; Pedersen, Gert Frølund

Published in:
I E E E Transactions on Microwave Theory and Techniques

DOI (link to publication from Publisher):
10.1109/TMTT.2020.2993307

Publication date:
2020

Document Version
Accepted author manuscript, peer reviewed version

Link to publication from Aalborg University

Citation for published version (APA):
Zhang, Y., Zhang, S., Yang, G., & Pedersen, G. F. (2020). A Wideband Filtering Antenna Array with Harmonic Suppression. *I E E E Transactions on Microwave Theory and Techniques*, *68*(10), 4327-4339. Article 9102359. https://doi.org/10.1109/TMTT.2020.2993307

General rights
Copyright and moral rights for the publications made accessible in the public portal are retained by the authors and/or other copyright owners and it is a condition of accessing publications that users recognise and abide by the legal requirements associated with these rights.

- Users may download and print one copy of any publication from the public portal for the purpose of private study or research.
- You may not further distribute the material or use it for any profit-making activity or commercial gain
- You may freely distribute the URL identifying the publication in the public portal -

Take down policy
If you believe that this document breaches copyright please contact us at vbn@aub.aau.dk providing details, and we will remove access to the work immediately and investigate your claim.

Downloaded from vbn.aau.dk on: December 06, 2025

A Wideband Filtering Antenna Array With Harmonic Suppression

Yi-Ming Zhang, *Member, IEEE*, Shuai Zhang, *Senior Member, IEEE*, Guangwei Yang, *Member, IEEE*, and Gert Frølund Pedersen

***Abstract*—In this work, a wideband 2×2 filtering antenna array is proposed and studied for fixed beam applications. The device is composed of a patch antenna array and a slotline-based four-way filtering power divider served as the feeding network. The integration of the antenna and the feeding parts is not a simple combination but a co-synthesis, where the characters of the two parts are both involved during the integration. First of all, the presented network is analyzed through an equivalent-circuit study to verify the frequency selectivity. Subsequently, integration synthesis of the network and the patch array is carried out to realize the filtering antenna array. For demonstration purposes, a filtering antenna array centered at 3 GHz is developed and fabricated. The measured absolute impedance bandwidth is 1.13 GHz, corresponding to a fractional bandwidth of 37.1%, and out-of-band rejection of up to 9.5 GHz is achieved. Compared to the array fed by a traditionally T-junction-based power divider, the absolute impedance bandwidth of the filtering array is significantly increased by 47%. The in-band gain of the proposed array is higher than 9.7 dBi, which is over 12.1 dBi from 2.75 GHz to 3.25 GHz. The results denote that compared to the previously reported literature the proposed filtering antenna array features: sharp cutoff response, wide impedance bandwidth, high gain as well as low cross-polarization level, with the harmonic suppression of up to three times the center frequency.**

***Index Terms*—Filtering antenna array, filtering power divider, harmonic suppression, differential feeding.**

I. Introduction

As TWO essential components/parts of modern wireless communication systems, the antenna and filter take significant roles for realizing the information exchanging purposes and stabling the system capacities. Because of the rapidly increasing demand for wireless services, growing efforts have been devoted to investigating the integration of filters and antennas, aiming to compactness, high frequency selectivity as well as a wideband response [1]-[19]. Moreover, harmonics and spurious signals generated in out-of-band frequencies are also critical issues, which would introduce severe interference between different frequencies. This denotes that the suppression of the undesired signals is of importance to the systems. To achieve the aforementioned filtering purposes, there are generally two approaches that are the antenna-filter fusion and filter synthesis approaches. The former focuses on the antenna design, hammering at the development of specified antenna configurations with filter-like responses [4]-[8]. The latter fastens on the filter design, where the characteristics of the required antennas are also involved during the design process [9]-[19].

As for the antenna-filter fusion approaches, the filtering response is mainly determined by the radiation structures [4]-[6]. In [4], a filtering dielectric resonator antenna was proposed. By introducing two microstrip stubs at the feeding point of the antenna, quasi-elliptic responses for impedance matching and realized gain are achieved. In [6], a wideband filtering antenna was reported, where additional slots were etched on the radiation patches to achieve the filtering purposes. The utilization of frequency selective surfaces is an alternative to develop filtering antennas, leading to bulky systems since the frequency selectivity surfaces are generally allocated with certain distances away from the antenna layers [7], [8]. The above schemes enable the feasibility of filtering antennas for single-antenna systems. However, facing to the antenna array applications where higher realized gains are required, these schemes might not be effective since additional resonances would be excited within the feeding network.

Using the filter synthesis approach would be more effective for filtering antenna array systems since the feeding networks of the arrays can be designed with filtering responses [11]-[17]. Please note that the filter synthesis approach is not just a connection of an antenna and a filter, but should be a comprehensive integration. Despite the increasing designs of filtering power dividers [20]-[22], the implementation of wideband filtering antenna arrays featuring high gain and wide stopband is still a challenge. This is because the impedance mismatching between the interfaces of feedings and antennas is unavoidable if the components are designed independently. A simple connection would lead to the degradation of the frequency selectivity of the whole system, especially at the frequency edges of passbands compared to the filters themselves [11], [12]. At this point, to overcome the mentioned issues, antennas should be considered as the final loads of the filtering networks, and the output impedance of the feeding networks is no longer matched to 50 Ω but some specified values.

In [11] and [13], two filtering power dividers were presented for 2×2 patch antenna arrays, respectively. With the specified

This work was supported by AAU Young Talent Program. (Corresponding author: *Shuai Zhang*)

The authors are with the Antenna, Propagation and Millimeter-wave Systems (APMS) Section, Department of Electronic Systems, Aalborg University, 9220 Aalborg, Denmark (e-mail: yiming@es.aau.dk; sz@es.aau.dk; guangweiy@es.aau.dk; gfp@es.aau.dk).

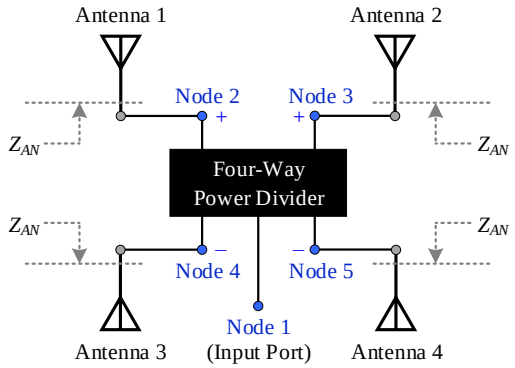

Fig. 1. Block diagram of a differential-fed 2×2 array with its feeding network.

feeding networks, filtering responses are achieved at the input ports of the arrays. Although the impedance bandwidth is increased in each case compared to the ones using traditionally T-junction-based feeding networks, but still features a narrow fractional bandwidth of 3%. In [12], a 2×2 filtering antenna array was proposed. With the developed loop-resonator-based filtering power divider, a high frequency selectivity was achieved. The second harmonic of the antenna array can be suppressed, and the measured fractional bandwidth is 5.6%. In [17], to enhance the impedance and axial ratio bandwidths, a filtering feeding network was provided and studied for a 2×2 circularly polarized antenna array. The measurement denotes a fractional bandwidth of 8.3 % with a maximum gain of 9.88 dBi. The aforementioned schemes enable the filtering responses of antenna arrays by designing filtering power dividers. Although sharp cutoffs are realized at frequency edges, the bandwidth features a narrow response. Besides, the in-band maximum gain of these cases is no more than 9.88 dBi, which characterizes a low level from a 2×2 array point of view.

In this paper, a wideband filtering antenna array consisting of a 2×2 patch antenna array and a four-way slotline-based filtering power divider is presented and studied for fixed beam applications. Although slotline-based components have been studied in recent years [23]-[29], these researches mainly focus on the in-band transmission performance and do not provide effective approaches for feeding 2×2 antenna arrays. On the other hand, the proposed power divider features compactness, out-of-phase output, high frequency selectivity as well as wide stopband, and can be utilized as the feeding network of antenna arrays. Further, by synthesizing the impedance characteristics of the proposed network and a 2×2 patch antenna array, a wideband and high-gain filtering antenna array is realized. Compared to recently published 2×2 filtering antenna arrays, the proposed scheme features wider impedance bandwidth, higher realized gain with an up to third-order harmonic suppression level, verified by both full-wave simulations and measurements.

This paper is organized as follows. Section II presents the theoretical synthesis of the proposed filtering antenna array configuration, including the analysis of the filtering network and the comprehensive integration of the network and the 2×2 antenna array. Besides, a simple design procedure of the

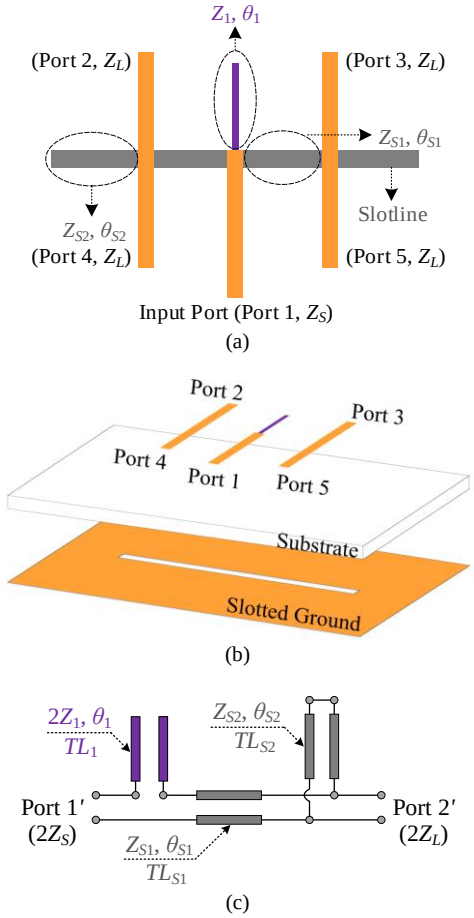

Fig. 2. Basic configuration (marked as Case A) of the proposed slotline-based four-way power divider, where $\theta_1 = \pi/2$ and $\theta_{S1} = \theta_{S2} = \pi/4$ referred to f_H. (a) Top view. (b) 3-D view. (c) Simplified equivalent circuit model of the power divider.

proposed filtering array is summarized. In Section III, the implementation analyses of two design examples involving a four-way power divider and a filtering antenna array centered at 3 GHz are provided. Section IV presents the performance discussions of the fabricated prototypes and the performance comparisons with other published schemes. A feasibility of the proposed scheme for beam scanning is also discussed. Finally, the conclusion of this work is stated in Section V.

II. Synthesis of the Proposed Filtering Antenna Array

The block diagram of a 2×2 antenna array and its feeding network is shown in Fig. 1. The array configuration features a mirror symmetry for the horizontal plane, requiring a differential feeding for broad-side radiation. Therefore, the network is designed to provide four outputs with out-of-phase, as illustrated in Fig.1 where Nodes 2 and 3 are positive, and Nodes 4 and 5 are negative. In this work, a slotline-based four-way power divider is proposed and served as the feeding of the array. Finally, a wideband filtering antenna array with harmonic suppression can be realized. For the input impedance Z_{AN} of every antenna element, it can be readily designed to 50 Ω at the center frequency. However, it would be extremely changed as the frequency departs from the center. This would degrade the filtering response of the system, especially at the

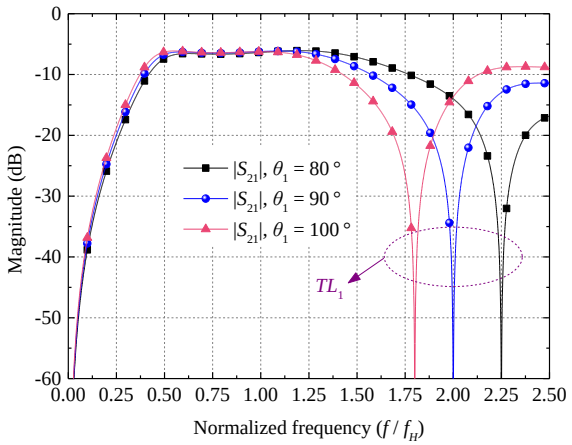

Fig. 3. Calculated transmission responses of the four-way power divider versus different values of θ_1 referred to f_H, based on Case A shown in Fig. 2(c). The source impedance and load impedance are set to the traditional values of $Z_S = Z_L$=50 Ω.

frequency edges once the power divider is developed independently of the antenna array. Therefore, it is not a simple connection of an antenna array and a bandpass filter by 50-Ω lines, but should be a comprehensive synthesis including the input/output impedance of the feeding network and the antenna array, as discussed in Section I.

The following discussion is started from a basic-structure study of the proposed slotline-based power divider. Further, the synthesis of the improved configuration is carried out to determine the final architecture of the power divider and achieve the performance of high frequency selectivity and harmonic suppression. The last part of this section focuses on the integration of the proposed power divider and a 2×2 patch antenna array, aiming at the realization of a wideband filtering antenna array.

A. Synthesis of differential four-way power divider

Shown in Figs. 2(a) and 2(b) is the basic configuration of the slotline-based four-way power divider. A slotline is loaded on the ground plane of a substrate layer. Three microstrip lines are printed on the other side of the substrate, serving as the input ports and output ports respectively. The source impedance and load impedance are marked as Z_S and Z_L, respectively. The electrical lengths of the transmission lines are fixed as mentioned in Fig. 2, while the characteristic impedances are the variables that will be determined later. It is readily found that the output Ports 2 and 4 are out-of-phase owing to the transmission characteristics of slotlines, which is similar for the Ports 3 and 5. Prior to the bandpass filter synthesis, a general setting involving the center frequency (f_0) and the lower and upper attenuation poles (f_L and f_H) of the passband is adopted, expressed as

$$f_0 = \frac{f_L + f_H}{2} \tag{1}$$

Owing to the symmetry, the magnitudes transmitting from Port 1 to the other four ports would be identical. Moreover, the output ports 2 and 4 would be out of phase due to the transmission characteristics of the slotlines, which is similar for ports 3 and 5. The simplified equivalent circuit is given in Fig. 2(c), where the transmission matrix M_1 can be derived according to network analysis, given as

$$M_1 = \begin{bmatrix} A_1 & B_1 \\ C_1 & D_1 \end{bmatrix} \tag{2a}$$

$$A_1 = \cos\theta_{S1} + \frac{2Z_1 \sin_{S1}}{Z_{S1}\tan\theta_1} + \frac{Z_{S1}\tan\theta_{S1}}{Z_{S2}\tan\theta_{S2}} - \frac{2Z_1\cos\theta_{S1}}{Z_{S2}\tan\theta_{S2}\tan\theta_1} \tag{2b}$$

$$B_1 = jZ_{S1}\sin\theta_{S1} - j\frac{2Z_1\cos\theta_{S1}}{\tan\theta_1} \tag{2c}$$

$$C_1 = j\frac{\sin\theta_{S1}}{Z_{S1}} - j\frac{\cos\theta_{S1}}{Z_{S2}\tan\theta_{S2}} \tag{2d}$$

$$D_1 = \cos\theta_{S1} \tag{2e}$$

It should be mentioned that the radiation of the slotline is unavoidable in practice due to its transmission characteristics. According to the studies in [23]-[29], the slotline radiation can be ignored during the transmission-line-based synthesis for slotline-based microwave components, since the in-band radiation loss is with a very low level, especially in sub-6 GHz applications. Therefore, the slotline radiation is not involved during filtering analysis. Further, the S parameters can be formulated based on the microwave network theory, expressed as [30]

$$S_{11} = S_{11,S} = \frac{2A_1Z_L + B_1 - 4C_1Z_S^*Z_L - 2D_1Z_S^*}{2A_1Z_L + B_1 + 4C_1Z_SZ_L + 2D_1Z_S} \tag{3a}$$

$$S_{21} = \frac{1}{4}S_{21,S} = \frac{\sqrt{R_SR_L}}{2A_1Z_L + B_1 + 4C_1Z_SZ_L + 2D_1Z_S} \tag{3b}$$

where S_{11} and S_{21} represent the S parameters of the four-way power divider shown in Fig. 2(a), $S_{11,S}$ and $S_{21,S}$ are the S parameters of the two-port circuit given in Fig. 2(c). The asterisk denotes the conjugate operation, and R_S and R_L represent the real part of the source and load impedance, respectively. Based on the aforementioned discussion, it is found that

$$\mathrm{Im}\left[2A_1Z_0 + B_1 + 4C_1Z_0^2 + 2D_1Z_0\right]\Big|_{f=2f_H} = \infty \tag{4}$$

Then, we have

$$S_{21}\big|_{f=2f_H} = 0 \tag{5}$$

This means that there would be a transmission zero at $f = 2f_H$ regardless of the load value. Besides, bandpass response can be obtained with specified values of Z_1, Z_{S1}, and Z_{S2} determined by synthesizing the derived S parameters given in (3). Here, graphical studies are operated based on the circuit model to show the transmission performance against normalized frequency (defined as the ratio of f and f_H), as plotted in Fig. 3. The simple analysis applied to the graphical studies in Fig. 3 gives a reasonable conclusion that the operating band of Case A would be involved in the range of $0.5f_H$ - f_H with a bandpass response, as expected. It is also clearly seen that the transmission zero is determined by the electrical length θ_1, and

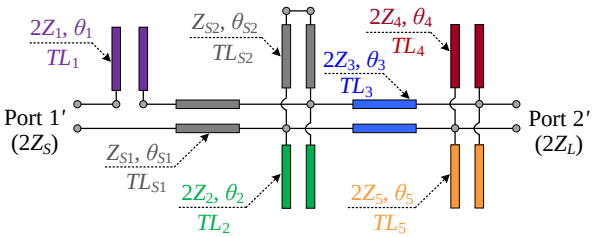

Fig. 4. Equivalent circuit model (marked as Case B) of the proposed slotline-based power divider with performance improvement compared to the one illustrated in Fig. 2(c), where $\theta_2 = \pi/2$ referred to f_H, $\theta_3 = \pi/4$ referred to f_H, $\theta_4 = \pi/2$ referred to f_L, and $\theta_5 = \pi/3$ referred to f_H.

there is no transmission zero at lower frequencies except DC with a narrow stopband response at higher frequencies.

Since the network model illustrated in Fig. 2 does not present the desired performance, an improved configuration is further proposed to enhance the performance, especially the in-band impedance matching and stopband rejection levels, as shown in Fig. 4 and marked as Case B. Subsequently, the four-way power divider based on Case B is fully synthesized. By taking network analysis, the transmission matrix M_2 of the simplified two-port network plotted in Fig. 4 can be formulated as

$$M_2 = \begin{bmatrix} A_2 & B_2 \\ C_2 & D_2 \end{bmatrix} \tag{6a}$$

$$A_2 = jP_4\left[2Z_3\left(P_1P_2+P_3\right)\sin\theta_3 - P_1\cos\theta_3\right] + \left(P_1P_2+P_3\right)\cos\theta_3 + \frac{P_1\sin\theta_3}{2Z_3} \tag{6b}$$

$$B_2 = -jP_1\cos\theta_3 + j2Z_3\left(P_1P_2+P_3\right)\sin\theta_3 \tag{6c}$$

$$C_2 = P_4\cos\theta_3\cos\theta_{S1} + j\frac{\cos\theta_{S1}\sin\theta_3}{2Z_3} - jP_5\cos\theta_3 - 2Z_3P_4P_5\sin\theta_3 \tag{6d}$$

$$D_2 = \cos\theta_3\cos\theta_{S1} - 2Z_3P_5\sin\theta_3 \tag{6e}$$

where

$$P_1 = \frac{2Z_1\cos\theta_{S1}}{\tan\theta_1} - Z_{S1}\sin\theta_{S1} \tag{7a}$$

$$P_2 = \frac{\tan\theta_2}{2Z_2} - \frac{1}{Z_{S2}\tan\theta_{S2}} \tag{7b}$$

$$P_3 = \cos\theta_{S1} + \frac{2Z_1\sin\theta_{S1}}{Z_{S1}\tan\theta_1} \tag{7c}$$

$$P_4 = \frac{\tan\theta_4}{2Z_4} + \frac{\tan\theta_5}{2Z_5} \tag{7d}$$

$$P_5 = \frac{\sin\theta_{S1}}{Z_{S1}} + \frac{\cos\theta_{S1}\tan\theta_2}{2Z_2} - \frac{\cos\theta_{S1}}{Z_{S2}\tan\theta_{S2}} \tag{7e}$$

Then, we have

$$S_{11,F} = S_{11,\,Case\,B} = \frac{2A_2Z_L + B_2 - 4C_2Z_S^*Z_L - 2D_2Z_S^*}{2A_2Z_L + B_2 + 4C_2Z_SZ_L + 2D_2Z_S} \tag{8a}$$

$$S_{21,F} = \frac{1}{4}S_{21,\,Case\,B} = \frac{\sqrt{R_SR_L}}{2A_2Z_L + B_2 + 4C_2Z_SZ_L + 2D_2Z_S} \tag{8b}$$

where $S_{11,F}$ and $S_{21,F}$ represent the S parameters of the four-way power divider based on Case B, $S_{11,\,Case\,B}$ and $S_{21,\,Case\,B}$ are the S parameters of Case B.

Seeing that $\theta_2 = \pi/2$ referred to f_H, it can be derived that

$$S_{21,Case\,B}\big|_{f=f_H} = S_{21,Case\,B}\big|_{f=2f_H} = 0 \tag{9}$$

This indicates that an additional transmission zero is generated by introducing the open-circuited stub TL_2 at f_H. Similarly, due to the setting of $\theta_4 = \pi/2$ referred to f_L, it is derived that

$$\begin{aligned} S_{21,Case\,B}\big|_{f=f_H} &= S_{21,Case\,B}\big|_{f=2f_H} \\ &= S_{21,Case\,B}\big|_{f=f_L} = S_{21,Case\,B}\big|_{f=3f_L} = 0 \end{aligned} \tag{10}$$

The result denotes that transmission zeros are both generated at frequency f_L and $3f_L$. Furthermore, if we properly set $f_L = 0.5f_H$, we then have

$$\begin{aligned} S_{21,Case\,B}\big|_{f=0.5f_H} &= S_{21,Case\,B}\big|_{f=f_H} \\ &= S_{21,Case\,B}\big|_{f=1.5f_H} = S_{21,Case\,B}\big|_{f=2f_H} = 0 \end{aligned} \tag{11}$$

This result shows that transmission zeros are both observed at the lower and upper attenuation poles. Moreover, the second harmonic at $1.5f_H$ referred to center frequency f_0 is well suppressed. On the other hand, since the shunt stubs TL_1, TL_2, and TL_4 are employed for transmission-zero generation purposes at specified frequencies, high-impedance lines can be utilized for these stubs. Then, the impedance matching is mainly determined by the parameters θ_3, Z_3, Z_{S1}, Z_{S2}, and Z_5.

Based on the aforementioned discussions, the values of all parameters except θ_3, Z_{S1}, Z_{S2}, Z_3, and Z_5 are already given/selected. The unspecified ones will be determined by the synthesis of the transmission-line-based bandpass response, leading to a quasi-equal-ripple frequency response in the passband. As studied in [31], the transmission coefficient of a two-port network with an equal-ripple response has the following relation

$$\left|S_{21,E}\right|^2 = \frac{1}{1+\varepsilon^2\cos^2\left(n\phi+q\xi\right)} \tag{12a}$$

$$\cos\phi = \frac{\cos\theta}{\cos\theta_{CL}} \tag{12b}$$

$$\cos\xi = \frac{\cos\theta}{\cos\theta_{CL}}\sqrt{\frac{1-\cos^2\theta_{CL}}{1-\cos^2\theta}} \tag{12c}$$

where n and q represent the number of the cascaded transmission sections, and the in-band transmission-zero order, which are $n = 2$ and $q = 2$ in this case, respectively. The parameter θ_{CL} is the equivalent electrical length at the lower cutoff frequency f_{CL}, and ε is determined by the passband ripple level, which are expressed as

$$\theta_{CL} = \frac{\lambda_{CH}\pi}{\lambda_{CH}+\lambda_{CL}} \tag{13a}$$

TABLE I
CALCULATED VALUES OF THE PARAMETERS OF CASE B

Parameters	Values	Parameters	Values
θ_1	$\pi/2$ @ f_H	Z_1	100 Ω
θ_2	$\pi/2$ @ f_H	Z_2	100 Ω
θ_3	$\pi/4$ @ f_H	Z_3	68.2 Ω
θ_4	$\pi/2$ @ f_L (f_H /2)	Z_4	110 Ω
θ_5	$\pi/3$ @ f_H	Z_5	43.5 Ω
θ_{S1}	$\pi/4$ @ f_H	Z_{S1}	112.1 Ω
θ_{S2}	$\pi/4$ @ f_H	Z_{S2}	109.7 Ω

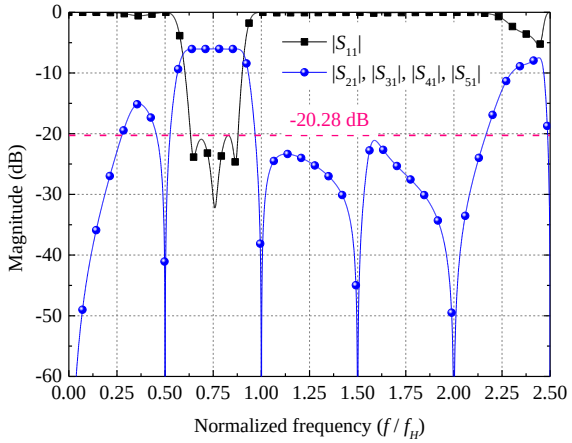

Fig. 5. Calculated *S* parameters of the four-port power divider based on Case B. The source impedance and load impedance are set to a traditional value of $Z_S = Z_L = 50$ Ω.

$$L_P = 10\log(1+\varepsilon^2) \tag{13b}$$

where L_P denotes the in-band maximum insertion loss, and λ_{CL} and λ_{CH} are the wavelengths at the lower and higher frequency band edges (f_{CL} and f_{CH}), respectively. Further, we employ a difference parameter Δ, in dB, defined as

$$\Delta = -20\log\left|S_{21,\ Case\ B}\right| + 20\log\left|S_{21,\ C}\right| \tag{14}$$

For the two-port network given in Fig. 4, a quasi-equal-ripple response can be achieved in the passband under the requirement of the nonnegative determinant

$$\Delta_{\min} \geq 0, \quad f \in [f_{CL}, f_{CH}] \tag{15}$$

The aforementioned discussion implies that by selecting a group value of θ_3, Z_{S1}, Z_{S2}, Z_3, and Z_5 to fit the requirement of (15), good impedance matching performance in the passband can be achieved theoretically. Meanwhile, the transmission zeros at the out of band would not depart. Here, a group of solution can be readily found with the specified parameters of $n = q = 2$, $f_{CL} = 0.635f_H$, $f_{CH} = 0.865f_H$, and $L_P = 0.044$ dB (corresponding to an insertion loss of 20 dB), which are listed in Table I. Fig. 5 depicts the calculated *S* parameters of the four-way power divider based on the scheme of Case B and the requirement of (15). It is observed that the calculated response exhibits a high frequency selectivity and a wide stopband. The insertion loss is higher than 20.28 dB in the passband, with a rejection of more than 15 dB up to $2.223f_H$ ($3f_0$) is achieved at the stopband. Especially starting from the upper attenuation pole of the passband to $2.169f_H$, an out-of-band rejection of over 20 dB is achieved.

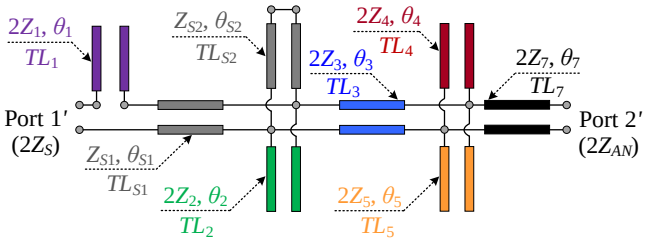

Fig. 6. Equivalent circuit model (marked as Case C) of the proposed slotline-based power divider for a 2×2 antenna array, where $Z_7 = 50$ Ω.

B. Discussion of a harmonic-suppressed filtering antenna array based on the proposed feeding network

The above synthesis is operated to verify the performance of the proposed filtering power splitter, where the source and loads are set as the traditional impedance of 50 Ω. However, if the proposed network is simply connected to a 2×2 antenna array by some 50-Ω transmission lines, the frequency selectivity response would be probably degraded. This is due to the mismatching between the output ports of the network and the antenna array, especially at the frequency edges of the filtering network, as discussed before. Therefore, to realize a filtering antenna array integrated with the presented filtering network, the impedance of the array and the additional 50-Ω transmission line should be taken into consideration.

Fig. 6 depicts the simplified equivalent circuit of the final configuration of an array integrated with the filtering network. The load impedance is replaced by the two times the antenna impedance, and a transmission line is connected between the load and the network. Referring to Case B shown in Fig. 4, the load impedance can be written as

$$2Z_L = 2Z_7 \frac{Z_{AN} + j2Z_7 \tan\theta_7}{2Z_7 + jZ_{AN} \tan\theta_7} \tag{16}$$

By substituting (16) into (8), the impedance matching performance of the array integrated with the power divider based on Case B can be easily calculated. Consequently, following the discussions of (12)-(14) to find an available group value of the parameters, a 2×2 array with filtering performance and harmonic suppression can be realized.

To describe the realization of the 2×2 filtering antenna array more clearly, a simple design procedure is summarized as follows:

Step 1: Determining the values of θ_1, θ_2, and θ_4. Based on the original specification including the center frequency, edges, and transmission zeros at specified frequencies, the mentioned parameters can be calculated, as studied in (5), (9)-(11).

Step 2: Calculating the impedance responses of the antenna array without any feeding. The responses can be readily obtained by using a full-wave electromagnetic (EM) simulator.

Step 3: Determining the values of Z_{S1}, Z_{S2}, Z_3, Z_5 and θ_3. Based on the impedance responses obtained in *Step* 2 and (6)-(8), (16), the transmission response of Case C can be

evaluated with a given group of Z_{S1}, Z_{S2}, Z_3, Z_5, θ_3. Estimating and checking whether the values satisfy the nonnegative condition of (15). If not, renewing the values until they fit (15). Please note that the value of θ_7 is generally specified prior to starting this step since the physical configuration of the antenna array and all the electrical lengths of the transmission lines are already determined. This step is used for realizing a quasi-equal-ripple response in the passband and can be readily achieved by using a circuit simulator.

Step 4: Determining the final layout. Once the original values of the feeding network are determined through the *Steps* 1-3, the initial layout of the filtering antenna can be constructed. Finally, the layout will be numerically optimized by using EM simulations to achieve the required performance in practice.

Please note that the proposed filtering feeding network is not a simple cascade or combination of microstrip-line-to-slotline transitions and filtering stubs, but a highly integrated approach with comprehensive co-synthesis. This work is different from the existed slotline-based microwave components as reported in [23]-[29]. First of all, the open-circuited stub TL_1 is served not only for in-band impedance matching purposes but also for tuning the transmission zero in out of band in this work. Secondly, the 90°-stubs TL_2 and TL_4 benefit both the sharp cutoff at the frequency edges and the improvement of harmonic suppression level. Thirdly, owing to the specified configuration, several in-band poles are generated, leading to a well-designed impedance matching. Finally, a very high frequency selectivity still holds for a 2×2 antenna array integrated with the proposed feeding network, where the characteristic impedance of all the adopted transmission lines should be involved during the integration. The aforementioned features and merits are discussed for the first time and not mentioned or investigated in the previous studies of slotline-based microwave components.

In summary, by following the above design procedure and the discussions in this section, a 2×2 filtering antenna array with a high frequency selectivity and a wide stopband can be developed. Next, two design prototypes are provided. Results based on full-wave simulation and measurement are both discussed and summarized.

III. Analysis of Implementation

For verification purposes, two design examples are presented in this section. More specifically, a four-way power divider centered at 3 GHz and a wide 2×2 antenna array integrated with the proposed network are developed and discussed for implementation, respectively.

A. Implementation of the proposed power divider

Fig. 7 illustrates the physical layout of the developed four-way power divider, based on the proposed design procedure. The slotline is loaded on the ground plane, and the microstrip lines are printed on the top of the substrate Rogers RO4350B with the thickness and permittivity of 0.508 mm and 3.66, respectively. In this case, meandered microstrip lines are employed for miniaturization purposes, where mitered bends

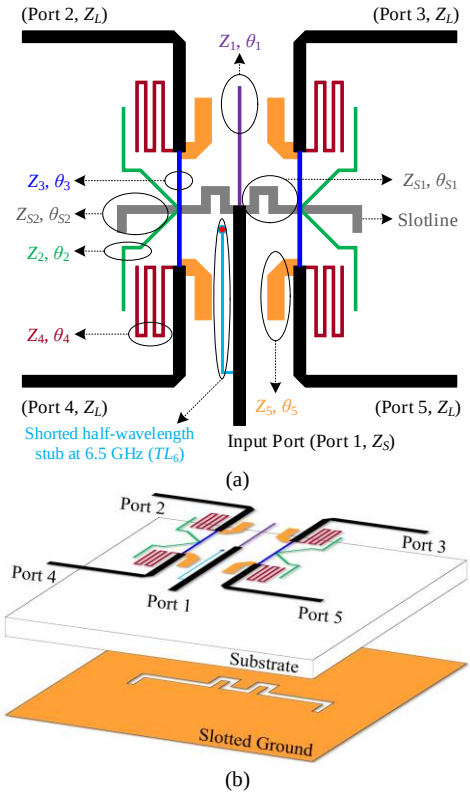

Fig. 7. Final layout of the proposed four-way power divider. (a) Plane layout, (b) 3-D view.

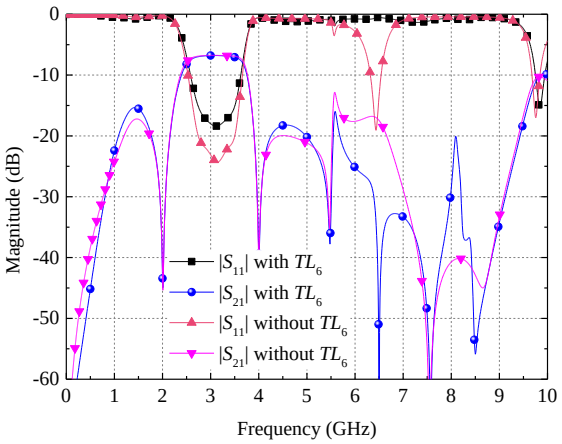

Fig. 8. Full-wave simulated *S* parameters of the developed four-way power divider with/without the stub TL_6.

are introduced based on the study in [32] to reduce the influence of the discontinuity. According to the investigations in [27] and [28], the slotline can be meandered as well, with nearly no change in the transmission performance. The full-wave simulated transmission responses are shown in Fig. 8. It is observed that the simulated results are consistent with the calculated ones depicted in Fig. 5 in the passband and around the frequency edges. Harmonic-suppressed response of up to $2f_0$ is achieved. However, two spurious resonances generated in the stopband degrade the stopband rejection, especially the one around 6.5 GHz. This is probably caused by the slotline radiation, which is not involved in the equivalent-circuit synthesis but does exist in real implementation.

The proposed filtering power divider is a preferable choice in

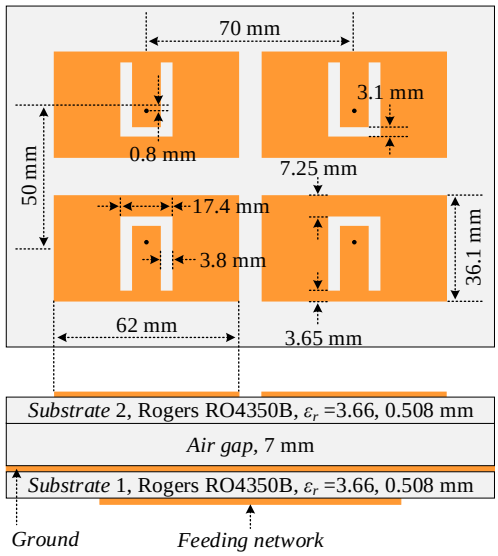

Fig. 9. Configuration of the 2×2 wideband patch antenna array.

the sub-6 GHz application since the radiation of the slotline is not high. Seeing that the slotline radiation still exists and would increase as the frequency increases, the higher harmonics suppression level would be degraded in practice, resulting from the increased radiation losses. In order to suppress the slot radiation, a shorted half-wavelength stub referred to 6.5 GHz is additionally introduced at the input interface of the network, marked as TL_6 and noted in Fig. 7. The stub TL_6 is with a high characteristic impedance of 115 Ω to avoid a significant effect on the circuit performance. Note that the contribution of the stub TL_6 is not taken into account during the design of the power divider as derived in Section II. This stub is simply added at the input port when the design of Case D is finished. It can be found from Fig. 8 that after integrating the stub TL_6, the spurious resonance is well suppressed. Despite some degradations on the impedance matching response in the passband, the overall performance of the power divider loaded with the stub TL_6 features a high frequency selectivity and wide stopband, as expected. The full-wave simulated results will be further discussed along with measured ones in Section IV.

B. 2×2 antenna array integrated with the proposed network

Since the purpose of this work is to present a filtering antenna array, a 2×2 wideband antenna array consisting of four U-slotted patch elements is employed and integrated with the proposed power divider. The physical configuration of the array is plotted in Fig. 9. Two substrates are stacked, and an air layer is inserted between the two substrates to achieve a wide impedance response. The radiation patches and the feeding network based on the proposed scheme are printed on the top of substrate 2 and bottom of substrate 1, respectively. The center distances between the vertical and horizontal pairs of elements are 50 mm and 70 mm respectively, corresponding to $0.5\lambda_0$ and $0.7\lambda_0$ (λ_0 is the free-space wavelength at 3 GHz).

By utilizing the EM simulator, the input impedance at each element port of the array without the feeding network can be readily observed. By following the design procedure provided in Section III, the values of all parameters can be determined. In this case, an available group of values is listed in Table II. Different from the first prototype where the output ports are designed for 50-Ω terminations, the output impedance of the feeding network is redesigned to achieve a good selectivity at band edges after integrating with the antenna array. Fig. 10 shows the calculated response of the array integrated with the proposed equivalent circuit Case C. It is observed that excellent filtering response is obtained, involving a very sharp cutoff at each frequency edge and a wide rejection band. Please note that for the calculated results, the additional stub TL_6 is not utilized, since this is a theoretical analysis and the slotline radiation is not involved. The stub TL_6 will be loaded in the practical implementation, and the full-wave simulated and measured results of the array will be provided in the next section.

TABLE II
CALCULATED VALUES OF THE PARAMETERS OF CASE D

Parameters	Values	Parameters	Values
θ_1	$\pi/2$ @ f_H	Z_1	81.4 Ω
θ_2	$\pi/2$ @ f_H	Z_2	109.4 Ω
θ_3	$\pi/4$ @ f_H	Z_3	117.2 Ω
θ_4	$\pi/2$ @ f_L ($0.5f_H$)	Z_4	106 Ω
θ_5	$\pi/3$ @ f_H	Z_5	60 Ω
θ_{S1}	$\pi/4$ @ f_H	Z_{S1}	109.2 Ω
θ_{S2}	$\pi/4$ @ f_H	Z_{S2}	121.2 Ω

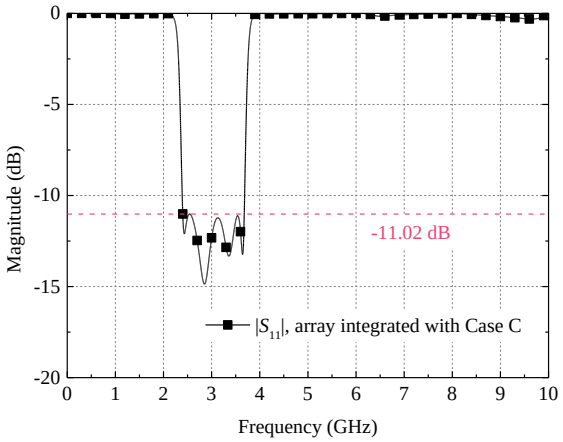

Fig. 10. Calculated impedance matching performance of the 2×2 antenna array integrated with the proposed power divider based on Case D.

IV. MEASUREMENTS AND DISCUSSIONS

A. Differential four-way power divider

Fig. 11 illustrates the photos of the fabricated four-way power divider with filtering and harmonic suppression responses. The physical size is 40 × 40 mm^2, corresponding to $0.4\lambda_0$ × $0.4\lambda_0$ at the center frequency of 3 GHz. The performance of the power divider is fully tested by using the Keysight Network Analyzer N5227A.

The measured *S* parameters of the power divider are plotted in Fig. 12(a), against the simulated ones. It is found that the measured and simulated results are consistent with each other. Within the passband from 2.6 GHz to 3.4 GHz, the measured transmission coefficients of the four output ports are better than

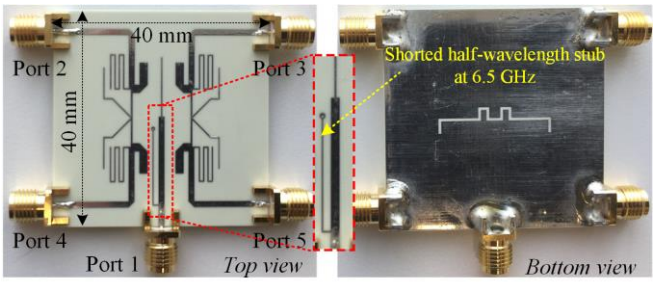

Fig. 11. Photos of the developed four-way feeding network.

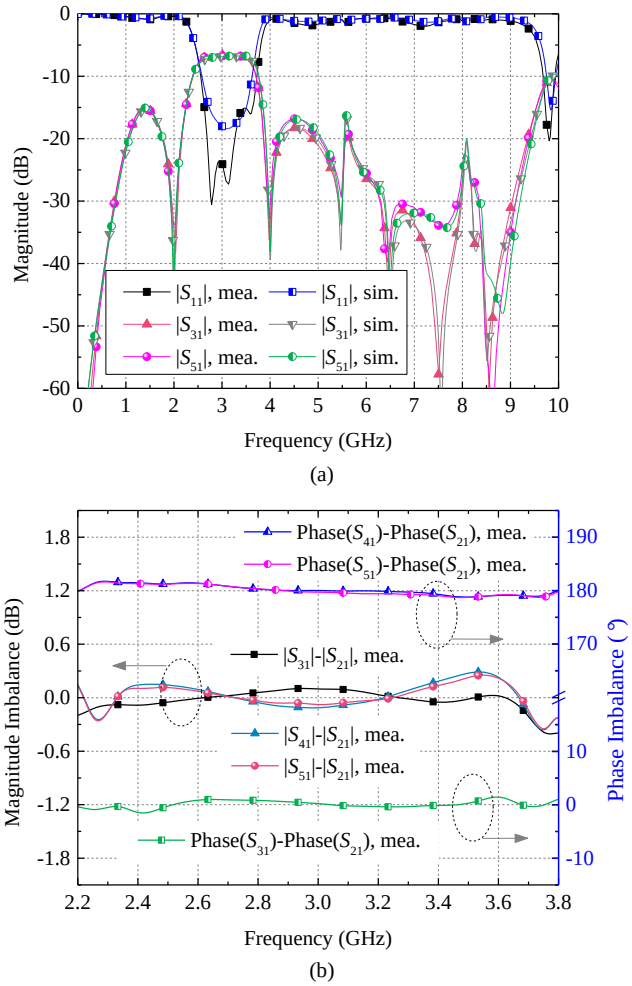

Fig. 12. Measured transmission responses of the developed four-way power divider. (a) *S* parameters. (b) Magnitude and phase imbalances.

TABLE III
COMPARISONS BETWEEN SOME PUBLISHED FILTERING POWER DIVIDERS AND THE PROPOSED ONE

Ref.	[12]	[14]	[21]	This work
Fractional bandwidth	~4.3%	~3.5%	6%	26.7%
Harmonic rejection	$2f_0$	No	No	$3f_0$
Differential output	Yes	Yes	No	Yes
Phase imbalance	/	/	/	±1.2 °
Magnitude imbalance	/	/	/	±0.17 dB

−7 dB, where the insertion loss introduced by the network is less than 1 dB. Moreover, it can be easily evaluated through

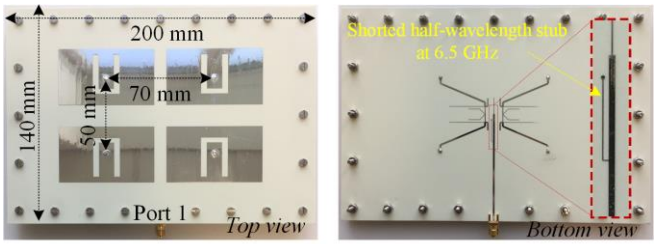

Fig. 13. Photos of the proposed 2×2 filtering antenna array.

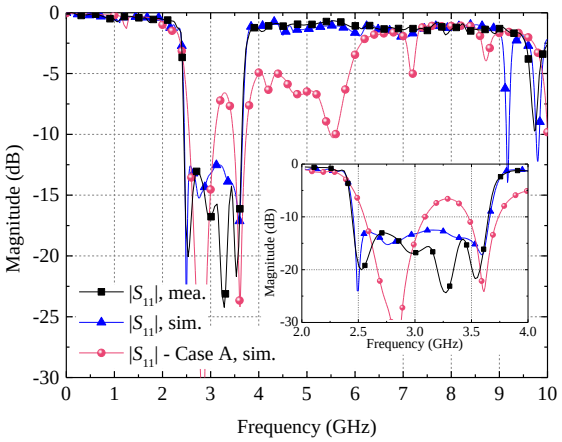

Fig. 14. Measured S_{11} of the proposed 2×2 filtering antenna array.

full-wave simulations that the insertion loss caused by the radiation of all transmission lines including the slotline is small of around 0.41-0.58 dB. Transmission zeros at 2 GHz and 4 GHz are observed, and a wide stopband from 4 GHz to over 9.5 GHz is obtained, referred to $|S_{21}| \leq -15$ dB. The magnitude and phase imbalances are also tested, as shown in Fig. 12(b). Within the passband, the maximum magnitude error between each pair of the four output ports is ±0.17 dB. The phase imbalance between the in-phase ports is less than 1 °, and the one between the antiphase ports is ±1.2 °, featuring a well-designed differential-output function among a wide bandwidth. Table III lists some published power dividers with filtering responses for comparison purposes. According to the measurement, it is verified that the proposed four-way power divider characterizes a high frequency selectivity in the passband, a wide rejection band as well as small output imbalances.

Using the structure of Case A shown in Fig. 2 is also an alternative approach to realize the differential feeding for the antenna array but without the filtering function. It is reasonably concluded that the phase and magnitude imbalances of Case A would be as good as the proposed one shown in Fig. 12 due to the slotline. However, there are no filtering and harmonic-suppression responses, as analyzed in Section II. Visible comparisons of the arrays using the networks of Case A and Case B are carried out in this work, which will be detailed in the next section.

B. 2×2 filtering antenna array

The 2×2 array shown in Fig. 9 integrated with the proposed filtering feeding network is also fabricated and measured. The photos of the demonstrator are provided in Fig. 13, where a shorted circuit half-wavelength stub at 6.5 GHz is still

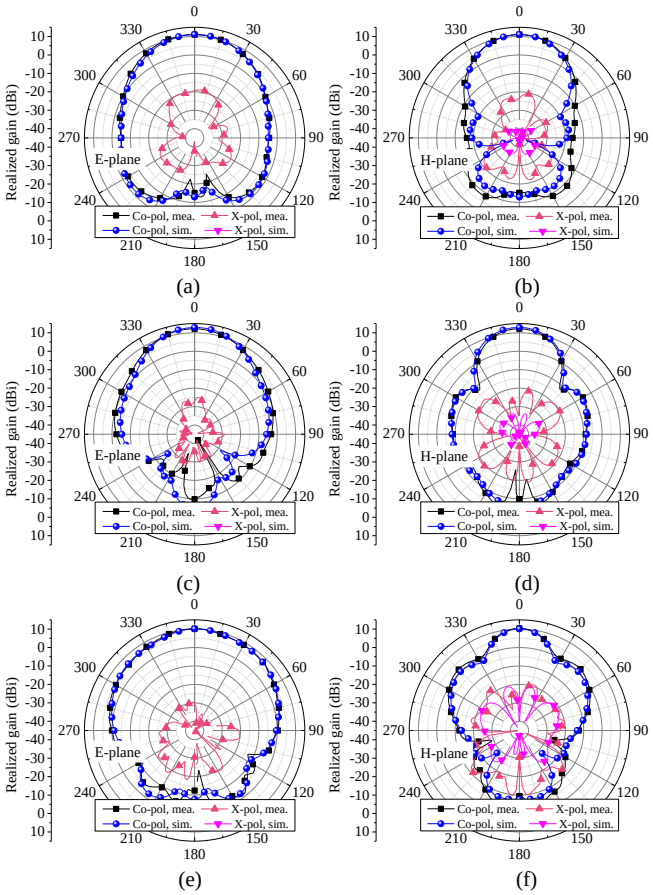

Fig. 15. Far-field radiation patterns of the proposed array. (a) 2.5 GHz, E-plane. (b) 2.5 GHz, H-plane. (c) 3.0 GHz, E-plane. (d) 3.0 GHz, H-plane. (e) 3.5 GHz, E-plane. (f) 3.5 GHz, H-plane.

employed to further suppress the slotline radiation.

Fig. 14 illustrates the measured and simulated impedance matching performance of the prototype. The simulated results of a 2×2 array integrated with the feeding network plotted in Fig. 2 are also given for comparison purposes. For the array integrated with Case A, the absolute impedance bandwidth (referred to $|S_{11}| \le -10$ dB) is 0.52 GHz from 2.56 GHz to 3.08 GHz, where several spurious within 3.5-6.0 GHz and around 7.2 GHz and 8.7 GHz are generated. After integrating the proposed filtering network, the impedance bandwidth (referred to $|S_{11}| \le -13$ dB) is markedly enhanced to 1.13 GHz from 2.48 GHz to 3.61 GHz, corresponding to a fractional bandwidth of 37.1%. Four reflection poles are generated in the passband, which is consistent with the numerical studies carried out in Section III. Moreover, a high frequency selectivity is realized, and the harmonics of up to 9.5 GHz (over $3f_0$) is well suppressed, as expected in the discussion of Fig. 10.

The far-field radiation patterns are fully tested as shown in Fig. 15, where the performance at 2.5 GHz, 3.0 GHz, and 3.5 GHz are provided, respectively. Please note that for the cross-polarized components at E-plane, discrepancy difference between the measured and simulated results is observed. Particularly, the simulated cross-polarization is not visible at E plane in Fig. 15 since the simulated results are less than −45 dB. This is mainly contributed by fabrication/assembling errors and

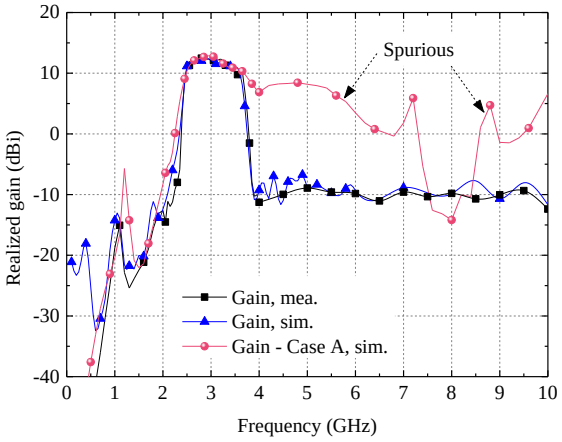

Fig. 16. Measured and simulated realized gains at boresight direction.

limited measurement accuracy in practice. Despite that, a low cross-polarization level of less than −20 dB is obtained owing to the differential feeding. Fig. 16 describes the realized gain of the developed prototype. As for the traditional one, harmonic radiations of over 5.9 dBi and 4.7 dBi are generated at 7.2 GHz and 8.7 GHz, respectively. Besides, there exist some spurious radiations within the band less than 2 GHz. On the other hand, it is found that for the array integrated with the proposed feeding network, a sharp roll-off is observed with a good stopband rejection level, and two nulls are observed at the two sides of the passband around the lower and higher frequency edges. The maximum realized gain of the array without filtering is 12.88 dBi at 2.95 GHz, while the one of the array with the filtering network is slightly dropped to 12.4 dBi at 2.9 GHz for both simulated and measured results. Seeing that the arrays with and without the filtering are well-matched around 2.9 GHz, the degradation of the realized gain mainly results from the integration with the filtering feeding. Despite a small drop of 0.48 dB in maximum gain, the in-band total efficiency of the filtering antenna array is still higher than 80.3%. Especially from 2.75 GHz to 3.25 GHz (representing a fractional bandwidth of 16.7%), the realized gain is over 12.04 dBi with a total efficiency of higher than 82%. The gain in the stopband is suppressed to less than −8.9 dBi. As for the stopband of less than 2 GHz, the out-of-band gain is also well-suppressed to smaller than −10 dBi.

C. Packaging and comparison study

Since slotline is utilized in the proposed scheme, the package requirement of the feeding network might be different from the ones using microstrip-line-based filtering approaches. Particularly, the performance of the filtering antenna might suffer from a small distance between the slotline and the inner surface of the package, leading to distortion/deterioration on the filtering performance. Here, a metal shield is loaded on the bottom side of the filtering antenna array to further investigate the performance of the scheme with a package, as illustrated in Fig. 17(a). The distance between the bottom side of substrate 1 and the inner face of the shield is $0.09\lambda_0$ (9 mm) where λ_0 is the free space wavelength referring to 3 GHz. The full-wave

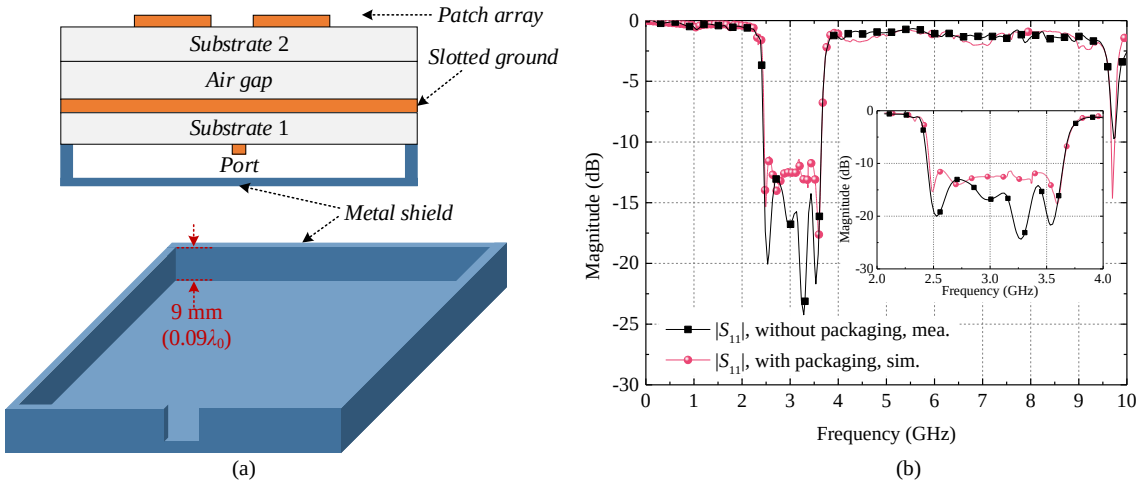

(a) (b)

Fig. 17. (a) Configuration of the antenna array with a metal shied. (b) *S*-parameter comparisons.

TABLE IV
COMPARISONS BETWEEN SOME PUBLISHED 2×2 FILTERING ANTENNA ARRAYS AND THE PROPOSED ONE

Ref.	Fractional bandwidth	Total profile height	In-band gain	In-band total efficiency	Spurious rejection level	Attenuation between in-band and out-of-band gains	Maximum in-band cross-polarized gain
[11]	3.0%	$0.0085\lambda_0$	≤ 9.6 dBi	~72.2%	$1.12f_0$	24.6 dB	−12.0 dBi
[12]	5.6%	$0.018\lambda_0$	≤ 9.7 dBi	Not given	$2.2f_0$	22.5 dB	−10.7 dBi
[14]	3.5%	$0.019\lambda_0$	≤ 8.3 dBi	~58.3%	$1.14f_0$	22.0 dB	−18.0 dBi
[17]	8.3%	$0.134\lambda_0$	≤ 9.88 dBi	~83.0%	$1.8f_0$	13.0 dB	−15.12 dBi
This work	37.1%	$0.08\lambda_0$	9.7~12.4 dBi	> 80.3%	$3f_0$	18.6 dB	−18.2 dBi

simulated *S* parameters of the antennas with and without the shield are depicted in Fig. 17(b). Despite that the transmission response is slightly changed when the shield is loaded, high frequency selectivity and good spurious suppression remain. The results denote that the proposed structure can be packaged by using a metal shield with a small height of $0.09\lambda_0$. This is of importance for some applications where the breakage of the ground is not preferred. Besides, the radiation performance is close to each other for the proposed antennas without and with the shield, which is not detailed for brevity.

For comparison purposes, some published 2×2 filtering antenna arrays are summarized, as tabulated in Table IV along with the proposed one. Here, we mainly focus on the bandwidth, profile, in-band gain as well as out-of-band gain suppression. The fractional bandwidths of these schemes feature a narrow response. It is clearly seen that the presented array in this work exhibits a much wider bandwidth than the other schemes, with a higher in-band realized gain. As for the antenna array reported in [17], the improved impedance bandwidth is contributed by the sequentially rotated array configuration, which is still less than 10%. It is also verified that a wide spurious band of up to three times the center frequency is achieved by using the proposed scheme. The total profile height of the developed demonstrator is $0.08\lambda_0$, which is much larger than the ones of [11], [12], and [14]. The high profile is utilized for realizing the wideband antenna. It is seen from Fig. 14 that the wide filtering bandwidth is contributed by both the proposed feeding network and the wideband antenna. As for the published works listed in Table III, it can be reasonably evaluated that a narrow band filtering feeding network generally cannot extend the impedance bandwidth dramatically even though wideband antennas are employed.

Note that the attenuation between in-band and out-of-band gains is around 18.6 dB, 3.4-6.0 dB less than those in [11], [12], and [14]. On the other hand, in terms of the recommendation of unwanted emissions in the spurious domain provided by the International Telecommunication Union [33] and the 3rd Generation Partnership Project [34], a normally higher than 43 dB is required for the out-of-band rejection, compared to the in-band total mean power. It is difficult to achieve such a quite strict attenuation for array applications under a single approach, according to the literature survey. Although the proposed scheme does not achieve the requirement directly, it can significantly reduce the burden of subsequent rejections. A potential solution is the combination of the antenna-filter fusion and filter synthesis approaches, where antenna and filtering feeding network are both designed with harmonic suppression function. In further, we will focus on the design of the antenna and its integration synthesis with filtering feeding networks to further improve the spurious suppression level. This would be a challenge since the desired antenna needs to fit the requirement of bandwidth, harmonic suppression, and especially the feasibility of the integration with filtering feedings.

D. Feasibility for beam scanning

In the published literatures as mentioned above, filtering

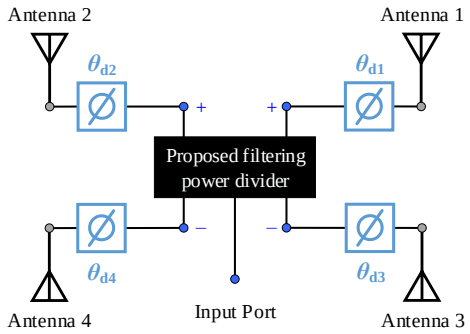

Fig. 18. Architecture used for investigating the scanning performance of the array integrated with the proposed filtering network. Different phase delays (θ_{d1}, θ_{d2}, θ_{d3}, and θ_{d4}) are employed between the output ports of the feeding network and the antenna elements for beam scanning purposes.

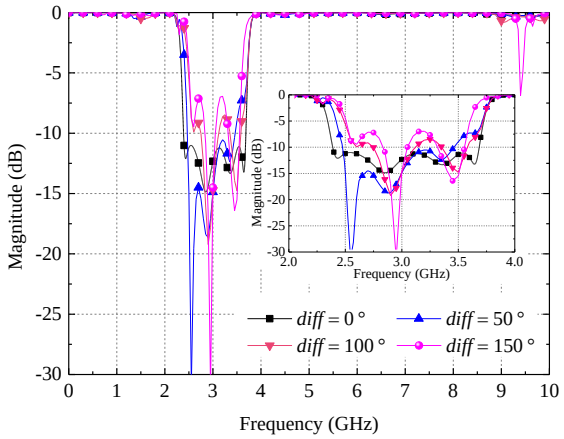

Fig. 19. Calculated transmission responses of the array shown in Fig. 18 with different phase shifter values of *diff* between θ_{d1} and θ_{d3} after integrating with the proposed filtering network.

antenna arrays were generally developed for fixed beam applications, the beam scanning performance was not considered. Here, discussions of the feasibility of the proposed approach for beam scanning is further carried out. For wide-angle scanning purposes, a large phase difference between antenna elements is always essential for excitation. In practice, owing to the common issue that the active impedance matching of the antenna elements might be significantly changed during the scanning due to the mutual coupling among the antennas.

Fig. 18 illustrates the configuration of the array integrated with the proposed filtering feeding network with some additional phase delays (θ_{d1}, θ_{d2}, θ_{d3}, and θ_{d4}) for beam scanning purposes. Based on the synthesis study given in Section II, the reflection coefficient of the filtering array can be readily calculated. In this part, the beam scanning performance along *x*-axis is studied, and it is set that $\theta_{d1} = \theta_{d2}$ and $\theta_{d3} = \theta_{d4}$. The filtering network is determined by the parameters listed in Table II. Fig. 19 presents the calculated *S* parameters of the filtering antenna arrays shown in Fig. 18, under several phase differences of 0 °, 75 °, and 150 ° between θ_{d1} and θ_{d3}. Theoretically, a large phase difference between θ_{d1} and θ_{d3} would provide a wide beam scanning angle. It is found that under the scanning conditions, the impedance matching becomes worse, as we discussed before. Despite that, the in-band reflection coefficients are almost less than −6 dB, which is acceptable for wide-angle beam forming applications from the industrial requirement point of view. Moreover, the high frequency selectivity still holds with several in-band poles, and the out-of-band rejection are all kept as good as the one under broadside radiation. The aforementioned discussion denotes that the proposed approach provides a potential scenario for beam scanning systems with filtering response.

V. Conclusion

A filtering antenna array with wide impedance bandwidth, sharp cutoff response, and harmonic suppression is proposed and synthesized in this paper. First of all, a slotline-based four-way power divider with filtering response and differential output is presented. The transmission-line theory is utilized to operate the synthesis of the equivalent circuit and verify the performance of the power divider. It is investigated that the proposed scheme enables several transmission zeros at the two sides of the passband. Besides, the theoretical studies have shown that the transmission zeros at different frequencies are determined independently by different parts of the structure. This exhibits the feasibility of tuning the transmission zeros to several specified frequencies, and the operating frequency would not be departed. Subsequently, a 2×2 patch antenna array is employed and integrated with the proposed power divider. Since the output ports of the power divider and the input ports of the antenna elements are not well-matched especially in the stopband, the input impedance of the antenna elements is taken into account during the analysis and development of the power divider.

To further demonstrate the performance, two prototypes that are the four-way power divider and the 2×2 filtering array centered at 3 GHz are developed and measured. The results denote that the impedance bandwidth of the filtering array is wider than the proposed feeding network itself, and also much larger than the array using a slotline-based power divider without any filtering function. Besides, calculations and simulations are driven to present the filtering and harmonic suppression performance under packaging and the feasibility for beam scanning. In brief, the proposed filtering antenna array features a well-designed performance, such as a very high frequency selectivity with a sharp cutoff, a high in-band realized gain, and a harmonic suppression level of over three times the center frequency.

References

[1] M. Troubat, S. Bila, M. Thevenot, D. Baillargeat, T. Monediere, S. Verdeyme, and B. Jecko, “Mutual synthesis of combined microwave circuits applied to the design of a filter-antenna subsystem,” *IEEE Trans. Microw. Theory Tech.*, vol. 55, no. 6, pp. 1182-1189, Jun. 2007.

[2] Z. H. Jiang, M. D. Gregory, and D. H. Werner, “Design and experimental investigation of a compact circularly polarized integrated filtering antenna for wearable biotelemetric devices,” *IEEE Trans. Biomed. Circuits Syst.*, vol. 10, no. 2, pp. 328-338, Apr. 2016.

[3] H. Tang, J.-X. Chen, H. Chu, G.-Q. Zhang, Y.-J. Yang, and Z.-H, Bao, “Integration design of filtering antenna with load-insensitive multilayer balun filter.” *IEEE Trans. Compon., Packag., Manuf. Technol.*, vol. 6, no. 9, pp. 1408-1416, Sep. 2016.

[4] P. F. Hu, Y. M. Pan, X. Y. Zhang, and B. J. Hu, "A compact quasi-isotropic dielectric resonator antenna with filtering response," *IEEE Trans. Antennas Propag.*, vol. 67, no. 2, pp. 1294-1299, Feb. 2019.

[5] W. Yang, Y. Zhang, W. Che, M. Xun, Q. Xue, G. Shen, and W. Feng, "A simple, compact filtering patch antenna based on mode analysis with wide out-of-band suppression," *IEEE Trans. Antennas Propag.*, vol. 67, no. 10, pp. 6244-6253, Oct. 2019.

[6] S. J. Yang, Y. M. Pan, Y. Zhang, Y. Gao, and X. Y. Zhang, "Low-profile dual-polarized filtering magneto-electric dipole antenna for 5G applications," *IEEE Trans. Antennas Propag.*, vol. 67, no. 10, pp. 6235-6243, Oct. 2019.

[7] A. A.-Tamijani, K. Sarabandi, and G. M. Rebiz, "Antenna–filter–antenna arrays as a class of bandpass frequency-selective surfaces," *IEEE Trans. Microw. Theory Tech.*, vol. 52, no. 8, pp. 1781-1789, Aug. 2004.

[8] X. Yang, H. Luyen, S. Xu, and N, Behdad, "Design method for low-profile, harmonic-suppressed filter-antennas using miniaturized-element frequency selective surfaces," *IEEE Antennas Wireless Propag. Lett.*, vol. 18, no. 3, pp. 427-431, Mar. 2019.

[9] C.-H. Wu, C.-H. Wang, S.-Y. Chen, and C. H. Chen, "Balanced-to-unbalanced bandpass filters and the antenna application," *IEEE Trans. Microw. Theory Tech.*, vol. 56, no. 11, pp. 2474-2482, Nov. 2008.

[10] Y. Yusuf, and X. Gong, "Compact low-loss integration of high-Q 3-D filter with highly efficient antennas," *IEEE Trans. Microw. Theory Tech.*, vol. 59, no. 4, pp. 857-865, Nov. 2011.

[11] C.-K. Lin, and S.-J. Chung, "A filtering microstrip antenna array," *IEEE Trans. Microw. Theory Tech.*, vol. 59, no. 11, pp. 2856-2863, Nov. 2011.

[12] C.-X. Mao, S. Gao, T. Wang, Z. Wang, F. Qin, B. Sanz-Izquierdo, and Q.-X. Chu, "An integrated filtering antenna array with high selectivity and harmonics suppression," *IEEE Trans. Microw. Theory Tech.*, vol. 64, no. 6, pp. 1798-1805, Jun. 2016.

[13] A. K. Sahoo, R. D. Gupta, and M. S. Parihar, "A 2×2 integrated filter antenna array," *2017 11th European Conference on Antennas and Propagation (EUCAP)*, Paris, France, 2017, pp. 2205-2208.

[14] H.-T. Hu, F.-C. Chen, J.-F. Qian, and Q.-X. Chu, "A differential filtering microstrip antenna array with intrinsic common-mode rejection," *IEEE Trans. Antennas Propag.*, vol. 65, no. 12, pp. 7361-7365, Dec. 2017.

[15] F.-C. Chen, H.-T. Hu, R.-S. Li, Q.-X. Chu, and M. J. Lancaster, "Design of filtering microstrip antenna array with reduced sidelobe level," *IEEE Trans. Antennas Propag.*, vol. 65, no. 2, pp. 903-908, Feb. 2017.

[16] F.-C. Chen, J.-F. Chen, Q.-X. Chu, and M. J. Lancaster, "X-band waveguide filtering antenna array with nonuniform feed structure," *IEEE Trans. Microw. Theory Tech.*, vol. 65, no. 12, pp. 4843-4850, Dec. 2017.

[17] T. Li, and X. Gong, "Vertical integration of high-Q filter with circularly polarized patch antenna with enhanced impedance-axial ratio bandwidth," *IEEE Trans. Microw. Theory Tech.*, vol. 66, no. 6, pp. 3119-3128, Jun. 2018.

[18] J.-F. Qian, F.-C. Chen, Y.-H. Ding, H-T. Hu, and Q.-X. Chu, "A wide stopband filtering patch antenna and its application in MIMO system," *IEEE Trans. Antennas Propag.*, vol. 67, no. 1, pp. 654-658, Jan. 2019.

[19] R. E. Lovato, T. Li, and X. Gong, "Tunable filter/antenna integration with bandwidth control," *IEEE Trans. Microw. Theory Tech.*, vol. 67, no. 10, pp. 4196-4205, Oct. 2019.

[20] C. Zhu, J. Xu, and W. Wu, "Microstrip four-way reconfigurable single/dual/wideband filtering power divider with tunable frequency, bandwidth, and PDR," *IEEE Trans. Ind. Electron.*, vol. 65, no. 11, pp. 8840-8850, Nov. 2018.

[21] F.-J. Chen, L.-S. Wu, L.-F.,Qiu, and J.-F. Mao "A four-way microstrip filtering power divider with frequency-dependent couplings," *IEEE Trans. Microw. Theory Tech.*, vol. 63, no. 10, pp. 3494-3504, Oct. 2015.

[22] M. Yang, J. Wang, X. Wang, and W. Wu, "Design of wideband four-way filtering power divider based on SIW loaded square patch resonator," *Electron. Lett.*, vol. 55, no. 7, pp. 389-391, Apr. 2019.

[23] R. Li, S. Sun, and L. Zhu, "Synthesis Design of Ultra-Wideband Bandpass Filters With Composite Series and Shunt Stubs," *IEEE Trans. Microw. Theory Tech.*, vol. 57, no. 3, pp. 684-692, Mar. 2009.

[24] X. Guo, L. Zhu, J.-P. Wang, and W. Wu, "Wideband microstrip-to-microstrip vertical transitions via multiresonant modes in a slotline resonator," *IEEE Trans. Microw. Theory Tech.*, vol. 63, no. 6, pp. 1902-1909, Jun. 2015.

[25] X. Guo, L. Zhu, K.-W. Tam, and W. Wu, "Wideband differential bandpass filters on multimode slotline resonator with intrinsic common-mode rejection," *IEEE Trans. Microw. Theory Tech.*, vol. 63, no. 5, pp. 1587-1594, May 2015.

[26] Y.-M. Zhang and J.-L. Li, "A dual-polarized antenna array with enhanced interport isolation for far-field wireless data and power transfer," *IEEE Trans. Veh. Technol.*, vol. 67, no. 11, pp. 10258-10267, Nov. 2018.

[27] L. Yang, L. Zhu, W.-W. Choi, K.-W. Tam, R. Zhang, and J.-P. Wang, "Wideband balanced-to-unbalanced bandpass filters synthetically designed with Chebyshev filtering response," *IEEE Trans. Microw. Theory Tech.*, vol. 66, no. 10, pp. 4528-4539, Oct. 2018.

[28] L. Yang, L. Zhu, R. Zhang, J. Wang, W.-W. Choi, K.-W. Tam, and R. G.-Garcia, "Novel multilayered ultra-broadband bandpass filters on high-impedance slotline resonators," *IEEE Trans. Microw. Theory Tech.*, vol. 67, no. 1, pp. 129-139, Jan. 2019.

[29] Y.-M. Zhang, S. Zhang, J.-L. Li, and G. F. Pedersen, "A dual-polarized linear antenna array with improved isolation using a slotline-based 180 ° hybrid for full-duplex applications," *IEEE Antennas Wireless Propag. Lett.*, vol. 18, no. 2, pp. 348-352, Feb. 2019.

[30] D. A. Frickey, "Conversions between S, Z, Y, H, ABCD, and T parameters which are valid for complex source and load impedances," *IEEE Trans. Microw. Theory Tech.*, vol. 42, no. 2, pp. 205-211, Feb. 1994.

[31] H. J. Carlin, and W. Kohler, "Direct synthesis of band-pass transmission line structures," *IEEE Trans. Microw. Theory Tech.*, vol. 13, no. 3, pp. 283-297, May 1965.

[32] N. Feix, M. Lalande, and B. Jecko, "Harmonical characterization of a microstrip bend via the finite difference time domain method," *IEEE Trans. Microw. Theory Tech.*, vol. 40, no. 5, pp. 955-961, May 1992.

[33] "Unwanted emissions in the spurious domain," *Recommendation ITU-R SM.329-12*. https://www.itu.int/rec/R-REC-SM.329/en

[34] "Base Station (BS) radio transmission and reception (Release 16)," *3GPP TS 38.104 V16.2.0*. https://www.3gpp.org/DynaReport/38-series.htm

Yi-Ming Zhang (S'17-M'19) received the B.S. degree from Central China Normal University in 2008, the M.S. and Ph.D. degrees from University of Electronic Science and Technology of China in 2014 and 2019, respectively. From 2018 to 2019, he was a guest researcher with the Antenna, Propagation and Millimeter-wave Systems (APMS) Section, Aalborg University, Denmark, where he currently works as a Post Doctor. His current research interests include massive MIMO antenna decoupling, single-channel full-duplex antennas, and passive RF and microwave components.

Shuai Zhang (SM'18) received the B.E. degree from the University of Electronic Science and Technology of China, Chengdu, China, in 2007 and the Ph.D. degree in electromagnetic engineering from the Royal Institute of Technology (KTH), Stockholm, Sweden, in 2013. After his Ph.D. studies, he was a Research Fellow at KTH. In April 2014, he joined Aalborg University, Denmark, where he currently works as Associate Professor. In 2010 and 2011, he was a Visiting Researcher at Lund University, Sweden and at Sony Mobile Communications AB, Sweden, respectively. He was also an external antenna specialist at Bang & Olufsen, Denmark from 2016-2017. He has coauthored over 50 articles in well-reputed international journals and over 15 (US or WO) patents. His current research interests include: mobile terminal MMwave antennas, biological effects, CubeSat antennas, Massive MIMO antenna arrays, UWB wind turbine blade deflection sensing, and RFID antennas.

Guangwei Yang (M'19) received the B.E., M.S., and Ph.D. degrees in electronic engineering from Northwestern Polytechnial University, in 2012, 2015, and 2019, respectively. He holds a postdoctoral position with the Antenna, Propagation and Millimeter-wave Systems (APMS) Section, Aalborg University, Denmark. He serves as a Reviewer for all the IEEE and IET journals related to antennas. His recent research interests include microstrip antennas, wideband antennas, millimeter-wave array antennas, circularly polarized antennas, base station antennas, phased array antennas, reconfigurable antennas, scanning antenna, and EM periodic structure.

Gert Frølund Pedersen was born in 1965. He received the B.Sc. and E.E. (Hons.) degrees in electrical engineering from the College of Technology in Dublin, Dublin Institute of Technology, Dublin, Ireland, in 1991, and the M.Sc.E.E. and Ph.D. degrees from Aalborg University, Aalborg, Denmark, in 1993 and 2003, respectively. Since 1993, he has been with Aalborg University where he is a Full Professor heading the Antennas, Propagation and Millimeter-wave Systems LAB with 25 researchers. He is also the Head of the Doctoral School on wireless communication with some 40 Ph.D. students enrolled. His research interests include radio communication for mobile terminals especially small antennas, diversity systems, propagation, and biological effects. He has published more than 500 peer reviewed papers, 6 books, 12 book chapters and holds over 50 patents. He has also worked as a Consultant for developments of more than 100 antennas for mobile terminals including the first internal antenna for mobile phones in 1994 with lowest SAR, first internal triple-band antenna in 1998 with low SAR and high TRP and TIS, and lately various multiantenna systems rated as the most efficient on the market. He has worked most of the time with joint university and industry projects and have received more than 21 M$ in direct research funding. He is currently the Project Leader of the RANGE project with a total budget of over 8 M$ investigating high performance centimetre/millimetre-wave antennas for 5G mobile phones. He has been one of the pioneers in establishing over-the-air measurement systems. The measurement technique is now well established for mobile terminals with single antennas and he was chairing the various COST groups with liaison to 3GPP and CTIA for over-the-air test of MIMO terminals. He is currently involved in MIMO OTA measurement.